

A Quantum-Walk Representation of Color-Ordered MHV Scattering Amplitudes

Anirudh Verma¹ and C. M. Chandrashekar¹

¹*Quantum Optics & Quantum Information Laboratory,*

Dept. of Electronic Systems Engineering, Indian Institute of Science, Bengaluru 560012, India

We introduce a graph-theoretic framework for representing color-ordered maximally helicity violating (MHV) scattering amplitudes in quantum chromodynamics using coined quantum walks on permutation trees. Each root-to-terminal path corresponds to a distinct color ordering of the external gluons, while local transition amplitudes are assigned according to the spinor-product structure of the Parke–Taylor amplitudes. The walk evolves in coherent superpositions over permutation sectors, giving a dynamical picture of the underlying combinatorics. A quantum-channel formulation based on Kraus operators is also introduced to describe sector-resolved contributions, while a weighted collection operator coherently combines the terminal sectors at a common reference node. A quantum Fourier transform on the coin space is then employed to combine the encoded contributions into the corresponding color-decomposed amplitude. Together, these constructions establish a unified graph-based framework connecting permutation trees, quantum walks, and open quantum systems providing a framework for quantum algorithms to simulate scattering processes in quantum field theory. As an example, numerical results for low-point gluon amplitudes demonstrate that the proposed representation faithfully captures the characteristic Parke–Taylor structure and is consistent with analytical results.

I. INTRODUCTION

Scattering amplitudes play a central role in quantum field theory and high-energy physics, providing the fundamental quantities from which measurable cross sections and decay probabilities are computed [1–3]. In perturbative quantum chromodynamics (QCD), amplitudes involving many external gluons exhibit intricate combinatorial and algebraic structures arising from color degrees of freedom, gauge symmetry, and helicity dependence [4, 6]. Despite the large number of contributing Feynman diagrams, remarkable simplifications occur in specific helicity sectors, most notably in the maximally helicity violating (MHV) amplitudes discovered by Parke and Taylor [5]. These developments have led to modern approaches to scattering amplitudes based on spinor-helicity variables, recursion relations [9, 13], twistor methods, and geometric formulations [8, 10–12, 14], providing compact analytic expressions for color-ordered gauge-theory amplitudes.

The color decomposition of gluon scattering amplitudes separates the full amplitude into color structures and kinematic partial amplitudes [6, 10],

$$M_n = \sum_{\sigma} C_{\sigma} A_{\sigma}, \quad (1)$$

where (C_{σ}) denotes the color factor associated with a permutation sector and (A_{σ}) is the corresponding color-ordered partial amplitude. For MHV amplitudes, the Parke–Taylor formula expresses the kinematic contribution as

$$A(1^-, 2^+, \dots, k^-, \dots, n^+) = \frac{\langle 1, k \rangle^4}{\langle 12 \rangle \langle 23 \rangle \dots \langle n1 \rangle}, \quad (2)$$

where the denominator consists of an ordered cyclic product of spinor inner products [5, 11]. The dependence on particle ordering gives the color decomposition an

intrinsically combinatorial structure, with the number of color-ordered sectors growing factorially as the number of external particles increases.

Recent years have witnessed growing interest in applying ideas from quantum information to quantum field theory, including quantum algorithms for field-theoretic simulations, quantum representations of scattering processes, and quantum-computing approaches to high-energy physics [15–18]. More recently, highlighting the importance of quantum-information-based formulation of MHV amplitudes through quantum-circuit constructions and amplitude reconstruction algorithms [19] has been proposed. In their proposal, quantum-circuit framework for MHV scattering amplitudes in which color, helicity, momentum, and permutation information are encoded into quantum registers and manipulated through structured unitary operations, leading to a reconstruction of the color-decomposed scattering amplitude.

In contrast, the present work formulates a graph-based representation in which color-ordered sectors are associated with paths on a directed permutation tree rather than encoding the scattering problem into quantum registers and circuit operations. In the graph-based model, each root-to-terminal path corresponds to a unique ordering of the external particles, while the topology of the graph reflects the combinatorial structure of the color decomposition. Within this framework, coined quantum-walk dynamics generate coherent superpositions over permutation sectors, and local transition amplitudes are chosen according to the spinor-product structure of the Parke–Taylor amplitudes. Consequently, the ordered denominator structure of the color-ordered amplitudes is represented through successive transitions on the permutation graph. Furthermore, the present framework incorporates a quantum-channel formulation for sector-resolved amplitude extraction

and reconstructs the color-decomposed amplitudes using a weighted collection operator together with a quantum Fourier transform. These features provide a complementary graph-based and dynamical perspective to the circuit-based formulation of Ref. [19]. A detailed table with comparison between the present graph-based construction and the quantum-circuit formulation of Ref. [19] is presented in the appendix (Table VII).

The quantum walk formalism is an highly successful framework for modeling quantum quantum dynamics, such as neutrino oscillations [29, 30], Dirac equation different dynamics in both the low and high energy regime [26–28, 32], and for developing a wide range of quantum algorithms to model dynamics on complex quantum networks, graph exploration [20–25]. The experimental demonstration of quantum walk to simulate the Dirac equation [31] and as a powerful primitive for quantum computation [33] further strengthens the practical relevance of the quantum walk framework for modeling scattering behavior in field theory dynamics. Since quantum walk evolution is naturally defined on graph structures, they are well suited for describing systems in which combinatorial organization plays a fundamental role. Motivated by these developments and to provide an algorithmic framework which can be implemented on a quantum processors in near future, we present a coined quantum walk on the permutation tree to provide a dynamical representation of the color-ordering structure of MHV amplitudes.

To analyze the resulting graph dynamics, we introduce a quantum-channel formulation in which Kraus operators act on the terminal permutation sectors to extract sector-resolved quantities proportional to the squared color-ordered amplitudes ($|A_\sigma|^2$) [34–36]. This channel description complements the underlying unitary quantum-walk evolution and establishes a connection with graph-based quantum dynamics and open quantum walks [37]. We further introduce a weighted collection operator that coherently combines the terminal sectors at a common reference node while preserving their relative weights. A quantum Fourier transform acting on the coin space is then used to combine the encoded contributions into the corresponding color-decomposed scattering amplitude. This establishes a neat connection between scattering amplitudes, permutation trees, coined quantum walks, and quantum channels. Rather than viewing the color decomposition solely as an algebraic sum over permutations, it also provides a graph-theoretic representation in which the ordering structure is encoded in the geometry of the permutation tree and explored through quantum-walk dynamics. Numerical examples for low-point gluon amplitudes demonstrate that the resulting construction faithfully reproduces the characteristic Parke–Taylor structure and agrees with analytical calculations.

The remainder of the paper is organized as follows. In Sec. II we review the color decomposition of tree-level QCD amplitudes, the Parke–Taylor MHV amplitudes, and introduce the permutation-tree representation of the color-ordering structure. In Sec. III we develop the coined quantum-walk framework by constructing the directed permutation graph together with globally consistent edge labeling, local coin operators, and a unitary shift operator. Section IV demonstrates how the resulting quantum walk generates coherent superpositions over color-ordered permutation sectors and establishes the connection between the accumulated transition amplitudes and the Parke–Taylor denominator structure. In Sec. V we formulate the quantum-channel description, introduce the weighted collection operator and quantum Fourier transform for coherent amplitude reconstruction, and present the complete reconstruction algorithm. Finally, Sec. VI presents numerical demonstrations for representative low-point gluon scattering amplitudes together with comparisons to the corresponding analytical results.

II. QCD AMPLITUDES, PARKE–TAYLOR STRUCTURE AND PERMUTATION TREES

In the high-energy regime, $Q^2 \gg \Lambda_{\text{QCD}}^2$, the strong coupling becomes sufficiently small for perturbative calculations to be applicable [1, 4]. A generic tree-level QCD amplitude can be decomposed into color and kinematic contributions,

$$M_n = \sum_{\sigma} C_{\sigma} A_{\sigma}, \quad (3)$$

where C_{σ} are color factors and A_{σ} are color-ordered partial amplitudes. For pure gluon scattering, a convenient trace decomposition is given by [6, 7, 10]

$$M_n = g^{n-2} \sum_{\sigma \in S_{n-1}} \text{Tr}(T^{a_1} T^{a_{\sigma(2)}} \dots T^{a_{\sigma(n)}}) A(1, \sigma(2, \dots, n)). \quad (4)$$

This decomposition separates the group-theoretic color structure from the kinematic information while explicitly organizing the scattering amplitude according to permutations of the external particles. Consequently, the combinatorial structure of gluon scattering is naturally encoded in the set of color-ordered permutation sectors.

Among the different helicity configurations, the dominant tree-level contributions arise from the maximally helicity violating (MHV) sector [5, 6]. For an n -gluon process with two negative-helicity gluons, the corresponding Parke–Taylor amplitude takes the compact form

$$A(1^-, 2^+, \dots, k^-, \dots, n^+) = \frac{\langle 1k \rangle^4}{\langle 12 \rangle \langle 23 \rangle \dots \langle n1 \rangle}, \quad (5)$$

where $\langle ij \rangle$ denotes the spinor-helicity inner product [8, 10, 11]. Throughout this work, the first and the k -th

gluons carry negative helicity while the remaining gluons have positive helicity.

For a fixed color ordering $(1, \sigma(2), \dots, \sigma(n))$, the corresponding color-ordered amplitude can be written as

$$A_\sigma = \frac{\langle 1k \rangle^4}{\langle 1\sigma(2) \rangle \langle \sigma(2)\sigma(3) \rangle \cdots \langle \sigma(n)1 \rangle}. \quad (6)$$

The denominator consists of an ordered cyclic product of spinor inner products determined entirely by the chosen permutation. This ordered structure suggests a natural combinatorial representation in which each permutation is associated with a sequence of local transitions, while the complete denominator is obtained by successively traversing the corresponding ordering.

Motivated by this observation, we represent the set of color-ordered sectors using a permutation tree. Starting from a root node, new particles are recursively appended to generate all admissible partial orderings, producing a directed tree whose terminal nodes correspond to complete permutations. Each root-to-terminal path therefore uniquely represents a color-ordered sector of the scattering amplitude. Within this representation, the factorial growth of the permutation sectors is encoded directly in the graph topology rather than being treated as an explicit sum over permutations. The permutation tree therefore provides a natural graph on which quantum-walk dynamics can be defined, allowing coherent superpositions over different color orderings while preserving the underlying combinatorial structure of the amplitude.

III. QUANTUM WALK CONSTRUCTION

To formulate a quantum walk [20, 22, 23] that generates all color-ordered sectors of the scattering amplitude, we first establish the combinatorial structure of the permutation tree as a directed graph, fix a global labeling of its edges, and use that labeling to define both the coin and shift operators in a mutually consistent way.

Before introducing the formal graph-theoretic definitions, it is useful to describe the construction intuitively. For an n -gluon color-ordered amplitude, particle 1 is kept fixed while the remaining particles $\{2, \dots, n\}$ are arranged in every possible order. Rather than generating all complete permutations directly, we build them recursively.

The construction begins at the root node (1), representing the trivial partial ordering containing only the fixed particle. At each step, one particle that has not yet appeared is appended to the current sequence, thereby creating a child node. Repeating this procedure generates a directed tree whose vertices represent partial permutations and whose terminal nodes correspond to complete permutations of the remaining particles.

For example, in the four-gluon case the root node (1) has three children,

$$(1, 2), \quad (1, 3), \quad (1, 4),$$

since particles 2, 3, and 4 are all initially available. From the node (1, 3), particle 3 has already been used, so only particles 2 and 4 remain available, producing the children

$$(1, 3, 2), \quad (1, 3, 4).$$

Continuing recursively eventually generates all $(n-1)!$ complete color orderings.

This recursive construction naturally defines a graph on which a coined quantum walk can be performed. The role of the coin operator is to distribute quantum amplitude among the admissible outgoing edges according to the local spinor-product weights, while the shift operator propagates each coin component to the corresponding child node. Consequently, every root-to-terminal path accumulates the sequence of transition amplitudes associated with one particular color ordering.

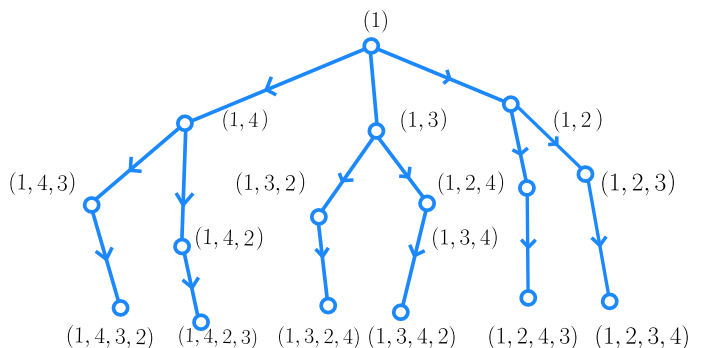


FIG. 1: Directed permutation tree for the four-gluon case. Each node represents a partial permutation $v = (1, a_2, \dots, a_m)$, while every directed edge corresponds to the append operation $v \rightarrow (v, a)$ for $a \in R(v)$. Every root-to-terminal path uniquely determines one complete color ordering of the external particles.

The recursive construction described above is illustrated in Fig. 1 for the four-gluon case. Every node represents a partial permutation beginning with the fixed particle 1, while every directed edge corresponds to appending one additional particle that has not yet appeared in the sequence. Since each particle is appended exactly once, every root-to-terminal path uniquely determines one complete color ordering of the external particles.

A. Directed graph and edge labeling

a. Global particle-to-coin map. Fix the set of external particles $\{1, 2, \dots, n\}$, where particle 1 is the reference particle. Define the *global particle-to-coin map*

$$c : \{2, \dots, n\} \rightarrow \{0, \dots, n-2\}, \quad c(j) = j-2. \quad (7)$$

This map is a bijection. Throughout this work, coin value k corresponds to particle $k+2$; this assignment is fixed and independent of the position of the walker on the graph.

b. Permutation tree as a directed graph. Define the directed graph $G = (V, E)$ as follows.

• **Vertex set.**

$$V = \{ (1, a_2, \dots, a_{m+1}) \mid 0 \leq m \leq n-1, a_i \in \{2, \dots, n\}, a_i \neq a_j \text{ for } i \neq j \}. \quad (8)$$

The unique node with $m = 0$ is the *root* $r = (1)$. Nodes with $m = n-1$ are *terminal*; denote their set $\mathcal{T} \subset V$. We have $|\mathcal{T}| = (n-1)!$ and $|V| = \sum_{k=0}^{n-1} (n-1)!/k!$.

• **Edge set.** There is a directed edge $v \rightarrow u$ whenever $u = (v, a)$ for some $a \in \{2, \dots, n\} \setminus \{a_2, \dots, a_{m+1}\}$. Write $\text{Out}(v)$ for the set of out-neighbors of v . Non-terminal nodes satisfy $|\text{Out}(v)| = n-1-m \geq 1$; terminal nodes satisfy $|\text{Out}(t)| = 0$.

c. Remaining-particle and placed-particle sets. For $v = (1, a_2, \dots, a_{m+1}) \in V$ define

$$R(v) = \{2, \dots, n\} \setminus \{a_2, \dots, a_{m+1}\}, \quad P(v) = \{a_2, \dots, a_{m+1}\}, \quad (9)$$

so that $\text{Out}(v) = \{(v, r) \mid r \in R(v)\}$, $|R(v)| = n-1-m$, and $R(v) \cup P(v) = \{2, \dots, n\}$.

d. Edge-label function (global). Using the global map (7), define the *edge-label function*

$$\lambda(v, (v, r)) = c(r) = r-2 \quad \text{for every } r \in R(v). \quad (10)$$

Thus each outgoing edge of v carries the *global* coin label of the particle it appends. Unlike a local labeling that renumbers remaining particles at each node, the label assigned to a particle is the same at every node where that particle is available. The outgoing edge labels at v therefore form the set $\{c(r) : r \in R(v)\} \subseteq \{0, \dots, n-2\}$, which in general is a proper subset of $\{0, \dots, n-2\}$: labels corresponding to already-placed particles are absent.

e. Incoming-coin function. For every non-root node $v = (1, a_2, \dots, a_{m+1}) \in V \setminus \{r\}$, define the *incoming coin label* as

$$\kappa(v) = c(a_{m+1}) = a_{m+1} - 2, \quad (11)$$

i.e. the global coin label of the *last appended particle*. For the root set $\kappa(r) = 0$ by convention (the walk is initialized with coin state $|0\rangle$).

The function κ is well-defined because every non-root node has a unique last element. It satisfies $\kappa(v) = \lambda(\text{par}(v), v)$ by construction, since the edge from $\text{par}(v)$ to v appends particle a_{m+1} and thus carries label $c(a_{m+1})$.

f. Example ($n = 4$). The global map is $c(2) = 0$, $c(3) = 1$, $c(4) = 2$. At the root: $R((1)) = \{2, 3, 4\}$, giving $\lambda((1), (1, 2)) = 0$, $\lambda((1), (1, 3)) = 1$, $\lambda((1), (1, 4)) = 2$. All three coin labels are present.

At node $(1, 3)$: $R((1, 3)) = \{2, 4\}$, $P((1, 3)) = \{3\}$, giving $\lambda((1, 3), (1, 3, 2)) = 0$ and $\lambda((1, 3), (1, 3, 4)) = 2$. The label set is $\{0, 2\}$; label 1 (corresponding to particle 3, already placed) is absent.

Incoming coin labels: $\kappa((1, 2)) = 0$, $\kappa((1, 3)) = 1$, $\kappa((1, 4)) = 2$.

The directed permutation tree corresponding to the four-gluon case is illustrated in Fig. 1. Each node represents a partial permutation beginning with the fixed particle 1, while each directed edge corresponds to appending one additional particle according to the graph construction described above. Every root-to-terminal path therefore represents one unique color ordering contributing to the scattering amplitude.

B. Hilbert space

The coined quantum walk can be described on the composite Hilbert Space consisting of

$$\mathcal{H} = \mathcal{H}_{\text{pos}} \otimes \mathcal{H}_{\text{coin}}, \quad (12)$$

where the *position space* is $\mathcal{H}_{\text{pos}} = \text{span}\{|v\rangle : v \in V\}$ and the *coin space* is $\mathcal{H}_{\text{coin}} = \text{span}\{|k\rangle : k = 0, \dots, d-1\}$ with

$$d = n-1. \quad (13)$$

A basis state $|v, k\rangle = |v\rangle \otimes |k\rangle$ represents the walker at node v with coin value k . For $n = 4$ we have $|V| = 16$, $d = 3$, and $\dim \mathcal{H} = 48$.

C. Coin operator

a. Local transition amplitudes. For each non-terminal node v and each out-neighbor $(v, r) \in \text{Out}(v)$ with $r \in R(v)$, define the *raw transition weight*

$$w(v, r) = \frac{1}{\langle \ell(v) | r \rangle}, \quad (14)$$

where $\ell(v)$ is the last particle label in the sequence v . Define the local normalization constant

$$\alpha_v = \sqrt{\sum_{r \in R(v)} |w(v, r)|^2}, \quad (15)$$

and the normalized amplitude

$$\tilde{v}_{v,r} = \frac{w(v, r)}{\alpha_v}. \quad (16)$$

By construction $\sum_{r \in R(v)} |\tilde{v}_{v,r}|^2 = 1$.

b. Local coin operator. For each non-terminal v , define a $d \times d$ unitary matrix $C_v \in U(d)$ satisfying the following column condition.

Let $\kappa(v)$ be the incoming coin label (defined in (11)). Require that the $\kappa(v)$ -th column of C_v encodes the normalized transition amplitudes, placed at the row corresponding to each remaining particle's global coin label:

$$(C_v)_{c(r), \kappa(v)} = \tilde{v}_{v,r} \quad \text{for every } r \in R(v), \quad (17)$$

with $(C_v)_{k, \kappa(v)} = 0$ for every $k \in \{c(a) : a \in P(v)\}$ (rows corresponding to already-placed particles are zero). The remaining $d-1$ columns of C_v are completed to a unitary matrix by Gram-Schmidt orthonormalization.

Remark 1 (Coin-shift consistency). When the walker arrives at v carrying coin state $|\kappa(v)\rangle$, the coin operator C_v maps $|\kappa(v)\rangle$ to a superposition $\sum_{r \in R(v)} \tilde{v}_{v,r} |c(r)\rangle$ over exactly those coin values whose corresponding particles are still available. The shift operator (defined below) then routes each component $|c(r)\rangle$ to the child (v, r) . In particular, the coin operator places zero amplitude in $|\kappa(v)\rangle$ itself (since particle $\kappa(v) + 2$ is already the last element of v and hence in $P(v)$), so the walker is always scattered away from the incoming coin direction.

For terminal nodes $t \in \mathcal{T}$, no forward transition is available; set $C_t = \mathbf{1}_d$ (identity).

c. Global coin operator. The full coin operator acts locally on each node:

$$C = \bigoplus_{v \in V} C_v \in U(d|V). \quad (18)$$

Its action on a basis state is $C|v, k\rangle = \sum_{j=0}^{d-1} (C_v)_{jk} |v, j\rangle$.

D. Shift operator

The shift operator S implements the conditional propagation of the walker along the directed edges of G [23, 25]. We define it as a permutation $\tau : V \times \{0, \dots, d-1\} \rightarrow V \times \{0, \dots, d-1\}$ and set $S|v, k\rangle = |\tau(v, k)\rangle$.

a. Partition of basis states. Fix a coin sector $k \in \{0, \dots, d-1\}$ and let $p = k+2$ denote the corresponding particle. Partition $V \times \{k\}$ into three disjoint sets:

$$F_k = \{(v, k) \mid v \notin \mathcal{T}, p \in R(v)\}, \quad (19)$$

$$L_k = \{(v, k) \mid v \notin \mathcal{T}, p \in P(v), k \neq \kappa(v)\}, \quad (20)$$

$$D_k = \{(v, k) \mid v \in \mathcal{T}\} \cup \{(v, k) \mid v \notin \mathcal{T}, k = \kappa(v), v \neq r\}. \quad (21)$$

F_k (*forward*) contains non-terminal states where particle p has not yet been placed. L_k (*loop*) contains non-terminal states where particle p has been placed but k is not the incoming coin label. D_k (*displaced*) contains all terminal states together with non-root states where k equals the incoming coin label (i.e. particle p was the last particle appended).

Remark 2 (Physical interpretation of D_k). A non-terminal state $(v, \kappa(v))$ falls in D_k rather than L_k because assigning it a self-loop would create a non-injectivity: the forward rule already maps $|\text{par}(v), \kappa(v)\rangle \rightarrow |v, \kappa(v)\rangle$, so a self-loop at $(v, \kappa(v))$ would give $|v, \kappa(v)\rangle$ two pre-images. Placing these states in D_k (alongside terminal states) and mapping them to otherwise-uncovered targets eliminates this conflict and makes S a bijection. During the first $n-1$ walk steps, these states are never populated because the coin operator always scatters the walker away from the incoming coin direction ($(C_v)_{\kappa(v), \kappa(v)} = 0$; see (17)), so they are dynamically equivalent to self-loops. This explains why the graph figures depict self-loop arrows at these positions.

b. Shift rules. The permutation τ is defined by:

$$\tau(v, k) = \begin{cases} ((v, k+2), k) & \text{if } (v, k) \in F_k \text{ (append} \\ & \text{particle } k+2), \\ (v, k) & \text{if } (v, k) \in L_k \text{ (self-loop),} \\ (\varphi_k(v), k) & \text{if } (v, k) \in D_k \text{ (displaced;} \\ & \text{reassignment),} \end{cases} \quad (22)$$

where φ_k is a bijection from the source set of D_k to the set \mathcal{U}_k of uncovered targets defined below.

For the four-gluon example, the partition

$$V \times \{k\} = F_k \cup L_k \cup D_k \quad (23)$$

can be evaluated explicitly for every node of the permutation tree. The complete classification of all basis states is provided in Appendix C. This explicit example illustrates how every basis state belongs to exactly one of the three subsets used in the construction of the unitary shift operator and serves as a direct verification of the algorithm presented above.

c. Uncovered targets. A state (w, k) is an *uncovered target* if it is neither a forward-rule image nor a self-loop fixed point:

$$\mathcal{U}_k = \{(w, k) \mid \kappa(w) \neq k \text{ or } w = r\} \setminus L_k. \quad (24)$$

A state (w, k) is a forward-rule image if and only if $\kappa(w) = k$ (the last element of w is particle $k+2$) and $w \neq r$. A state in L_k is its own image. The uncovered targets are everything else.

Proposition 1 (Bijectivity). $|D_k| = |\mathcal{U}_k|$ for every k , so a bijection $\varphi_k : D_k \rightarrow \mathcal{U}_k$ exists. The resulting map τ is a permutation on $V \times \{0, \dots, d-1\}$, and S is unitary.

Proof. The three source sets F_k, L_k, D_k partition $V \times \{k\}$. The forward rule is injective (each child has a unique parent per coin label), the self-loop rule is the identity on L_k , and φ_k is a bijection onto \mathcal{U}_k by definition. It remains to show the three image sets are disjoint.

- Forward images are states (u, k) with $\kappa(u) = k$ and $u \neq r$.

TABLE I: Summary of the notation used in the permutation-tree construction.

Symbol	Meaning
V	Set of vertices (partial permutations)
E	Set of directed edges
$r = (1)$	Root node
T	Set of terminal nodes (complete permutations)
$R(v)$	Remaining particles that have not yet appeared in v
$P(v)$	Particles already contained in v
$\text{Out}(v)$	Set of children of v
$c(j)$	Global particle-to-coin map
$\lambda(v, u)$	Coin label assigned to edge $v \rightarrow u$
$\kappa(v)$	Incoming coin label of node v
F_k	Forward states for coin value k
L_k	Loop states for coin value k
D_k	Displaced states used to complete the shift permutation
ϕ_k	Bijection completing the shift operator

The coined quantum-walk operator is

$$U = SC, \quad (26)$$

where C is the global coin operator (18) and S is the shift (22). After t steps the state of the walker is

$$|\psi_t\rangle = U^t |\psi_0\rangle = (SC)^t |\psi_0\rangle. \quad (27)$$

Since both C and S are unitary, U is unitary for all t . After $n - 1$ steps — the depth of the permutation tree — the walker reaches the terminal permutation sectors,

$$|\psi_{\text{fin}}\rangle = U^{n-1} |\psi_0\rangle = \sum_{\sigma \in S_{n-1}} \psi_\sigma |\sigma\rangle \otimes |\kappa_\sigma\rangle, \quad (28)$$

where each terminal node $\sigma = (1, \sigma(2), \dots, \sigma(n))$ uniquely labels a color-ordered permutation sector, and $\kappa_\sigma = c(\sigma(n)) = \sigma(n) - 2$ is the global coin label of the last appended particle. The derivation of the explicit form of the path amplitudes ψ_σ and their correspondence to the Parke–Taylor denominator is given in Appendix G.

IV. AMPLITUDE RECONSTRUCTION

The coined quantum walk on the permutation tree reconstructs the color-ordered Parke–Taylor amplitudes.

A. Reconstruction of Parke–Taylor Amplitudes

Starting from the initial state $|\psi_0\rangle = |(1)\rangle \otimes |0\rangle$ the walker evolves under repeated application of the coined quantum-walk operator $U = SC$ where C denotes the local coin operator and S is the conditional shift operator. After $n - 1$ steps, corresponding to the depth of

the permutation tree, the walker reaches the terminal permutation sectors, $|\psi_{\text{fin}}\rangle = (SC)^{n-1} |\psi_0\rangle$. As shown in Appendix G, the repeated action of the local coin and shift operators generates a coherent superposition over every root-to-terminal path,

$$|\psi_{\text{fin}}\rangle = \sum_{\sigma \in S_{n-1}} \psi_\sigma |\sigma\rangle \otimes |\kappa_\sigma\rangle, \quad (29)$$

where each terminal node uniquely labels a permutation sector.

The path amplitudes are derived in Appendix E by tracking the product of coin-matrix entries accumulated along each root-to-terminal path. The result is

$$\psi_\sigma = \frac{1}{\prod_{r=1}^{n-1} \alpha_{\sigma(r)}} \cdot \frac{1}{\langle 1 \sigma(2) \rangle \langle \sigma(2) \sigma(3) \rangle \cdots \langle \sigma(n) 1 \rangle}, \quad (30)$$

where $\alpha_{\sigma(r)}$ are the local normalization constants defined in (15). Comparing with the Parke–Taylor amplitude (6), one obtains the explicit proportionality

$$\psi_\sigma = \frac{\langle \sigma(n) 1 \rangle}{\langle 1 \tilde{k} \rangle^4 \prod_{r=1}^{n-1} \alpha_{\sigma(r)}} A_\sigma, \quad (31)$$

so that $\psi_\sigma \propto A_\sigma$, with the proportionality constant fully determined by known kinematic factors. The detailed recursive derivation is presented in Appendix G.

B. Open Quantum-System Formulation

To extract the contribution of each terminal permutation sector, we construct the density operator

$$\rho = |\psi_{\text{fin}}\rangle \langle \psi_{\text{fin}}| \quad (32)$$

and introduce a collection of Kraus operators [34–36] acting on the terminal nodes, $K_\sigma = c_\sigma |\sigma\rangle \langle \sigma| \otimes I_{\text{coin}}$, where the coefficients c_σ are chosen such that $\sum_\sigma K_\sigma^\dagger K_\sigma \leq I$. The explicit form of c_σ is given in Appendix H, Eq. (F5). The corresponding completely positive trace-non-increasing map is $\rho' = \sum_\sigma K_\sigma \rho K_\sigma^\dagger$.

As shown in Appendix F, this channel removes coherences between different permutation sectors while preserving sector-resolved probabilities, yielding

$$\rho' = \sum_\sigma \frac{|A_\sigma|^2}{|M|^2 \prod_{r=1}^{n-1} |\alpha_{\sigma(r)}|^2} |\sigma\rangle \langle \sigma| \otimes |k_\sigma\rangle \langle k_\sigma|. \quad (33)$$

Using the proportionality relation (31), the diagonal entries satisfy

$$(\rho')_{\sigma\sigma} \propto |A_\sigma|^2, \quad (34)$$

establishing a direct correspondence between the quantum-walk probabilities and the squared Parke–Taylor amplitudes. This channel description complements the unitary walk evolution and establishes a connection with open quantum walks [37, 38].

V. COHERENT AMPLITUDE RECONSTRUCTION

The Kraus-channel construction extracts the individual Parke–Taylor contributions associated with each terminal permutation sector. To recover the full scattering amplitude, these sectors must be recombined coherently.

A. Physical origin of the weighted collection operator

The need for a separate collection step arises from a structural asymmetry between the kinematic and color contributions to the scattering amplitude. The kinematic structure — the ordered cyclic product of spinor brackets forming the Parke–Taylor denominator — is *local*: each factor $\langle \ell(v) j' \rangle^{-1}$ depends only on the current node and the particle being appended. It is therefore accumulated naturally, edge by edge, during the quantum walk through the coin operator weights v_{v,u_j} . This is why the walk state $|\psi_{\text{fin}}\rangle$ already encodes the kinematic partial amplitudes A_σ (up to the normalization factors $\alpha_{\sigma(r)}$), as established in (31).

The color structure, by contrast, is *global*: the trace factor $\text{Tr}(T^{a_1} T^{a_{\sigma(2)}} \dots T^{a_{\sigma(n)}})$ depends on the *complete* permutation σ , not on any single edge. Consequently, color weights cannot be assigned locally during the walk — they require knowledge of the full root-to-terminal path, which is available only after the walker has reached a terminal node.

The weighted collection operator W^T resolves this asymmetry. It acts exclusively on the terminal sectors and performs two operations simultaneously: (i) it attaches the color weight $\text{Tr}(T^{a_1} T^{a_{\sigma(2)}} \dots T^{a_{\sigma(n)}})$ and any remaining kinematic correction to each permutation sector, and (ii) it transfers all terminal sectors to a common reference node R , enabling subsequent interference. The transfer to a common node is necessary because quantum-mechanical interference requires superposed amplitudes to occupy the same spatial mode; without collection, the amplitudes reside at distinct terminal nodes and cannot interfere.

After collection, all path-dependent information is stored in the coin degree of freedom. The coin state $|k_\sigma\rangle$ uniquely identifies which permutation sector contributed each amplitude, so a quantum Fourier transform on the coin space produces the coherent superposition required for the full color-decomposed amplitude.

B. Action on the terminal walk state

The explicit construction of W^T is given in Appendix I. Acting on the final walk state,

$$W^T |\psi_{\text{fin}}\rangle = |R\rangle \otimes \sum_{\sigma \in \mathcal{T}} c_\sigma |k_\sigma\rangle, \quad (35)$$

where

$$c_\sigma = \frac{\text{Tr}(T^{a_1} T^{a_{\sigma(2)}} \dots T^{a_{\sigma(n)}})}{\mathcal{N}} \frac{A_\sigma}{\prod_r \alpha_{\sigma(r)}}. \quad (36)$$

Remark 4 (Normalization factors). The coefficients c_σ contain the factor $1/\prod_r \alpha_{\sigma(r)}$, which varies across permutation sectors because the local normalization constants α_v depend on the spinor configuration at each node. These factors arise from the requirement that each local coin operator C_v be unitary: the physical transition amplitudes $w(v, u_j)$ are in general non-normalized, and the rescaling by α_v is the cost of embedding them into a unitary matrix. While these factors do not cancel in the coherent sum, they are fully determined by the input kinematics and can be computed classically in $O(n!)$ operations or absorbed into the normalization constant \mathcal{N} .

Remark 5 (Implementability of W^T). The weighted collection operator W^T is bounded ($|a_\sigma| \leq 1$) but not unitary, since it maps $|\mathcal{T}| = (n-1)!$ orthogonal terminal states to a single reference node. In a physical quantum implementation, W^T would need to be realized through an ancilla-assisted unitary dilation [36], embedding the non-unitary map into a larger unitary operator on an extended Hilbert space, followed by post-selection on the ancilla. The success probability of this post-selection decreases with the number of permutation sectors, which is a limitation shared by other amplitude-embedding approaches including the quantum circuit construction of Ref. [19].

Thus, all terminal permutation sectors are collected at the same reference node while the interference information remains encoded in the coin degrees of freedom. To recover the coherent sum over permutation sectors we apply the Quantum Fourier Transform (QFT) [36, 39] on the coin space and project onto the Fourier vacuum mode $|0\rangle$.

Remark 6 (Choice of mixing unitary). The reconstruction requires projecting onto a coin state that has uniform overlap with all coin basis states. Since $\langle 0|U_{\text{QFT}}|k\rangle = 1/\sqrt{d}$ for every k , the QFT followed by projection onto $|0\rangle$ produces an equal-weight coherent sum over all permutation sectors. Any $d \times d$ unitary whose first row is $(1/\sqrt{d}, \dots, 1/\sqrt{d})$ would achieve the same result; the QFT is adopted as the standard canonical choice.

The resulting coherent color-weighted sum satisfies

$$|\mathcal{M}_{\text{QW}}|^2 \propto \left| \sum_{\sigma \in S_{n-1}} \text{Tr}(T^{a_1} T^{a_{\sigma(2)}} \dots T^{a_{\sigma(n)}}) A_\sigma \right|^2. \quad (37)$$

The detailed derivation of the weighted collection operator, its action on the terminal walk state, and the Quantum Fourier Transform reconstruction are presented in Appendices I and J.

VI. NUMERICAL VALIDATION

In this section, we present numerical results for the four-gluon MHV scattering amplitude obtained using the quantum walk framework developed in the previous sections. The simulations serve three complementary purposes. First, they demonstrate the propagation of probability amplitude through the permutation tree. Second, they illustrate the extraction of sector-resolved Parke–Taylor weights through the Kraus-channel formulation. Finally, they validate the numerical reconstruction of the color-ordered scattering contributions.

A. Quantum Walk on the Permutation Tree

The walk is initialized at the root of the permutation tree according to

$$|\psi_0\rangle = |(1)\rangle \otimes |0\rangle, \quad (38)$$

where the first register labels the position of the walker on the permutation graph and the second register denotes the coin degree of freedom.

The evolution is generated through repeated applications of the unitary operator

$$U = SC, \quad (39)$$

where C denotes the local coin operation and S is the conditional shift operator. After t steps the state of the walker is

$$|\psi_t\rangle = U^t |\psi_0\rangle. \quad (40)$$

For the four-gluon case, the walker reaches the terminal sectors after three steps. Figure 1 shows the permutation tree employed in the simulations. Each root-to-terminal path corresponds to a unique color ordering.

The probability distribution at time t is obtained from

$$P_t(i) = \sum_c |\langle i, c | \psi_t \rangle|^2, \quad (41)$$

where i labels the position basis and c labels the coin state. The evolution of the walker probability distribution is shown in Fig. 3.

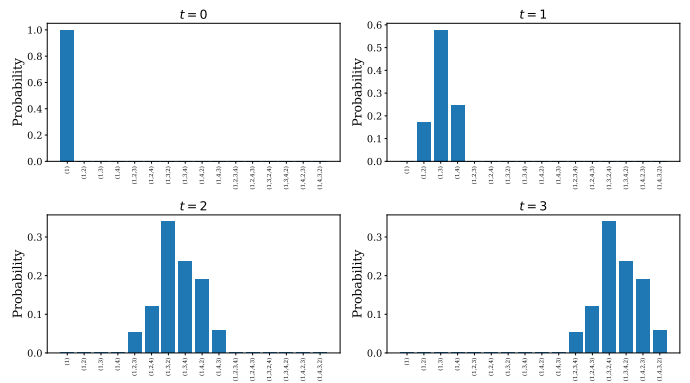


FIG. 3: Probability distribution of the quantum walker after successive applications of the evolution operator $U = SC$. The final step corresponds to the terminal permutation sectors.

B. Terminal Permutation Sectors

After three walk steps the state takes the form

$$|\psi_{\text{fin}}\rangle = \sum_{\sigma \in \mathcal{T}} \psi_{\sigma} |\sigma\rangle \otimes |k_{\sigma}\rangle, \quad (42)$$

where \mathcal{T} denotes the set of terminal permutation sectors and ψ_{σ} are the corresponding complex amplitudes.

The occupation probability associated with a terminal sector σ is

$$P(\sigma) = |\psi_{\sigma}|^2. \quad (43)$$

Figure 4 shows the resulting terminal-state distribution. Only terminal sectors possess nonzero probability, confirming that the walk correctly generates the complete set of color orderings.

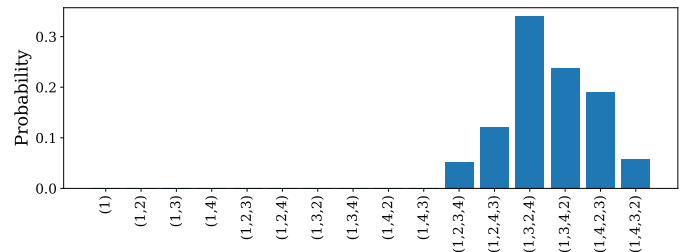


FIG. 4: Occupation probabilities of the terminal permutation sectors after completion of the quantum walk.

The amplitudes ψ_{σ} retain the relative phases accumulated during the walk and therefore encode the interference structure required for scattering-amplitude reconstruction.

C. Extraction of Parke–Taylor Weights

To extract sector-resolved probabilities we construct the density matrix

$$\rho = |\psi_{\text{fin}}\rangle \langle \psi_{\text{fin}}|. \quad (44)$$

Figure 5 shows the density matrix restricted to the occupied terminal sectors. The visible off-diagonal elements indicate coherence between different permutation sectors.

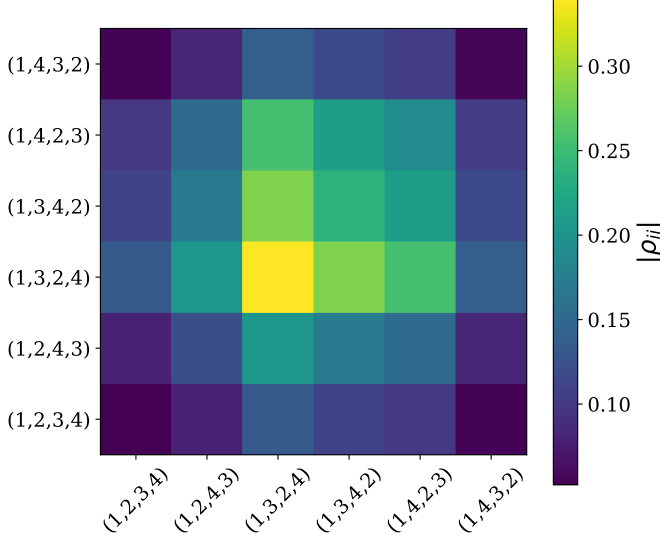


FIG. 5: Density matrix of the coherent terminal-state superposition before application of the Kraus channel.

The extraction channel is defined through

$$\rho' = \sum_{\sigma \in \mathcal{T}} K_{\sigma} \rho K_{\sigma}^{\dagger}, \quad (45)$$

where K_{σ} are the Kraus operators introduced in Sec. IV.

Application of the channel removes the inter-sector coherences while preserving the sector weights. The resulting density matrix is shown in Fig. 6.

The diagonal elements of the transformed density matrix satisfy

$$(\rho')_{\sigma\sigma} = \frac{|A_{\sigma}|^2}{|M|^2 \prod_{r=1}^{n-1} |\alpha_{\sigma(r)}|^2}, \quad (46)$$

where A_{σ} denotes the Parke–Taylor contribution associated with the permutation sector σ .

The extracted sector probabilities therefore provide direct access to the relative Parke–Taylor weights encoded within the quantum walk.

D. Numerical simulation of quantum walk and comparison with analytical amplitudes

The extracted sector weights are compared with the exact Parke–Taylor values in Fig. 7. Excellent agreement is observed across all six permutation sectors.

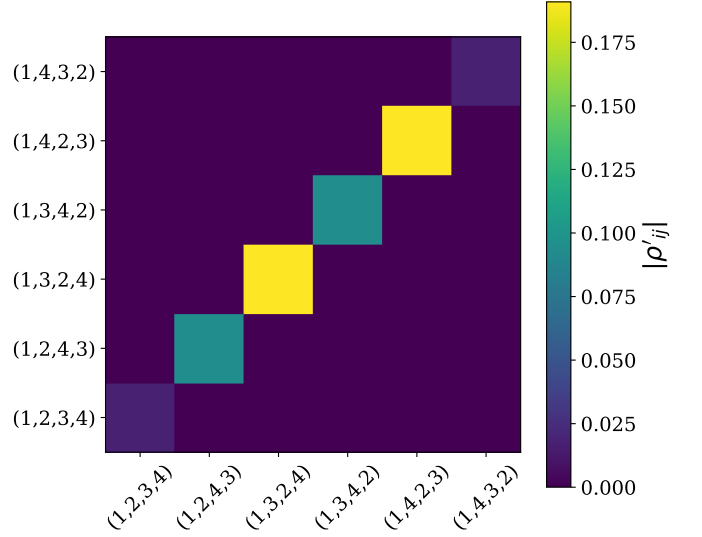


FIG. 6: Density matrix after application of the Kraus channel. The off-diagonal coherences are suppressed and only the sector probabilities remain.

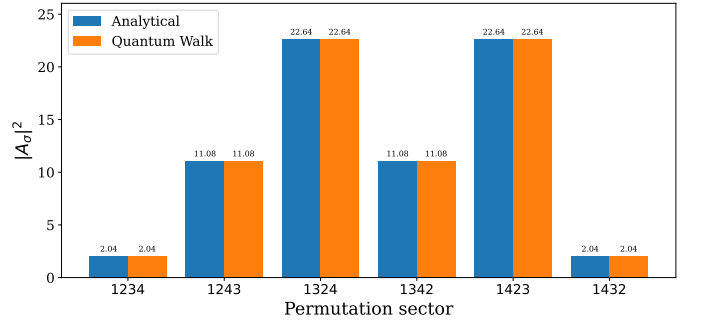


FIG. 7: Comparison between analytical Parke–Taylor weights and the values reconstructed from the quantum walk framework for all terminal permutation sectors.

The reconstructed values reproduce the analytical amplitudes with sub-percent relative error for every sector, demonstrating that the quantum walk correctly encodes both the combinatorial structure of the permutation tree and the associated kinematic weights.

E. Coherent Reconstruction of the Scattering Amplitude

The Kraus-channel formulation discussed above extracts the sector-resolved probabilities associated with the individual Parke–Taylor contributions. To recover the full scattering amplitude, the terminal permutation sectors must be recombined coherently.

Starting from the final walk state

$$|\psi_{\text{fin}}\rangle = \sum_{\sigma \in \mathcal{T}} \psi_{\sigma} |\sigma\rangle \otimes |k_{\sigma}\rangle, \quad (47)$$

we apply the weighted collection operator W^T , which maps all terminal sectors to a common reference node R while preserving their relative amplitudes.

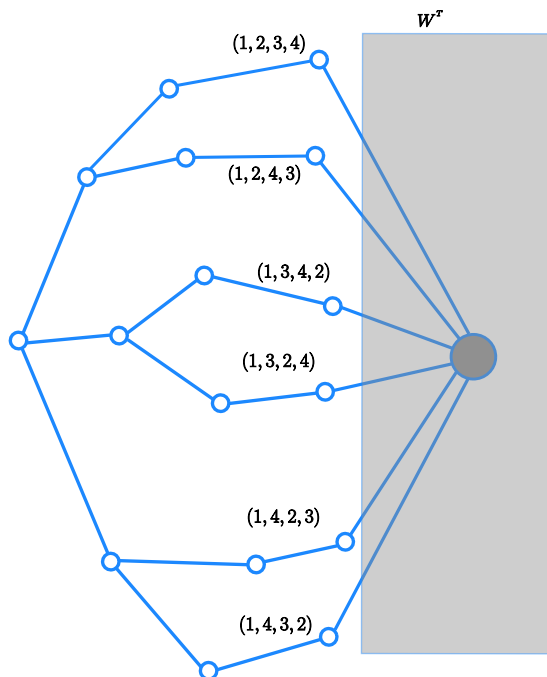


FIG. 8: Graphical representation of the weighted collection procedure. The terminal permutation sectors of the four-gluon permutation tree are coherently mapped to a common reference node R . The weights attached to each branch preserve the Parke–Taylor information and enable their subsequent interference.

The resulting state takes the form

$$W^T |\psi_{\text{fin}}\rangle = |R\rangle \otimes \sum_{\sigma \in \mathcal{T}} c_{\sigma} |k_{\sigma}\rangle, \quad (48)$$

where the coefficients c_{σ} contain the color and kinematic information associated with the corresponding permutation sector. As illustrated in Fig. 8, the collection operator maps all terminal sectors to a single reference node while preserving their relative weights.

To generate interference between the collected contributions, a quantum Fourier transform [36, 39] is applied to the coin space. For a coin dimension d , the Fourier operator is

$$U_{\text{QFT}} = \frac{1}{\sqrt{d}} \sum_{j,k=0}^{d-1} e^{2\pi i j k / d} |j\rangle \langle k|. \quad (49)$$

For the four-gluon example considered here, $d = 3$. The Fourier transform mixes the amplitudes stored in the coin basis and produces the coherent superposition required for amplitude reconstruction.

The reconstructed scattering amplitude is obtained by projecting onto the Fourier vacuum mode,

$$\mathcal{M}_{\text{QW}} = \sqrt{d} \langle 0 | U_{\text{QFT}} W^T |\psi_{\text{fin}}\rangle, \quad (50)$$

where the factor \sqrt{d} compensates for the normalization of the Fourier transform.

Remark 7 (Phase information). The projection formula (50) reconstructs the *complex* amplitude $\mathcal{M}_{\text{QW}} \in \mathbb{C}$. The relative phases between permutation sectors are preserved throughout the walk in the coin-space superposition, and are recovered by the QFT projection. The squared modulus $|\mathcal{M}_{\text{QW}}|^2$ is reported in Table II for comparison with analytical results, but the construction yields the full complex amplitude.

The resulting quantity corresponds to the coherent sum of the color-ordered contributions encoded in the quantum walk. Numerical evaluation confirms that the reconstructed amplitude agrees with the analytical Parke–Taylor result within numerical precision.

Quantity	Analytical	Quantum Walk
$ \mathcal{M} ^2$	0.05634	0.05634
Relative Error (%)	0.00	

TABLE II: Comparison between the analytical scattering amplitude and the value reconstructed from the quantum walk framework.

VII. CONCLUSION

We have introduced a quantum-walk representation of color-ordered gluon scattering amplitudes based on the permutation-tree structure underlying the Parke–Taylor formula. The construction maps the recursive generation of color orderings onto a discrete-time quantum walk defined on a permutation graph: coin operators encode local branching probabilities, while shift operators propagate amplitude through the tree, so that the resulting coherent walk state contains contributions from all color-ordered sectors simultaneously. A quantum-channel formulation was developed to extract the sector-resolved probabilities associated with individual Parke–Taylor contributions, and numerical simulations for four-gluon MHV amplitudes show excellent agreement with analytical results, confirming that the quantum walk faithfully reproduces the expected kinematic weights.

These results establish a connection between scattering amplitudes, quantum walks, and open quantum-system techniques and quantum network architecture. The quantum algorithmic framework of studying scattering amplitudes provides a quantum-information perspective to model, simulate and study such dynamics using quantum computers. Future directions include extensions to higher multiplicities, non-MHV amplitudes, loop corrections, and implementations using open quantum walks and quantum-network architectures.

-
- [1] M. E. Peskin, D. V. Schroeder, An Introduction to Quantum Field Theory, [Addison-Wesley \(1995\)](#)
- [2] Steven Weinberg, The Quantum Theory of Fields, Vol. I, [Cambridge University Press \(1995\)](#)
- [3] Matthew D. Schwartz, Quantum Field Theory and the Standard Model, [Cambridge University Press \(2014\)](#)
- [4] R. K. Ellis, W. J. Stirling, B. R. Webber, QCD and Collider Physics, [Cambridge University Press \(1996\)](#)
- [5] Stephen J. Parke, Thomas R. Taylor, An amplitude for n -gluon scattering, [Phys. Rev. Lett. **56**, 2459–2460 \(1986\)](#)
- [6] Michel L. Mangano, Stephen J. Parke, Multiparton amplitudes in gauge theories, [Phys. Rept. **200**, 301–367 \(1991\)](#)
- [7] Vittorio Del Duca, Lance J. Dixon, Frederick Maltoni, New color decompositions for gauge amplitudes at tree and loop level, [Nucl. Phys. B **571**, 51–70 \(2000\)](#)
- [8] Z. Xu, D. Zhang, L. Chang, Helicity amplitudes for multiple bremsstrahlung, [Nucl. Phys. B **291**, 392–428 \(1987\)](#)
- [9] F. A. Berends, W. T. Giele, Recursive calculations for processes with n gluons, [Nucl. Phys. B **306**, 759–808 \(1988\)](#)
- [10] Lance J. Dixon, Calculating scattering amplitudes efficiently, [TASI Lectures, hep-ph/9601359 \(1996\)](#)
- [11] Henriette Elvang, Yu-tin Huang, Scattering Amplitudes in Gauge Theory and Gravity, [Cambridge University Press \(2015\)](#)
- [12] Edward Witten, Perturbative gauge theory as a string theory in twistor space, [Commun. Math. Phys. **252**, 189–258 \(2004\)](#)
- [13] Ruth Britto, Freddy Cachazo, Bo Feng, Edward Witten, Direct proof of tree-level recursion relation in Yang–Mills theory, [Phys. Rev. Lett. **94**, 181602 \(2005\)](#)
- [14] Freddy Cachazo, Song He, Ellis Ye Yuan, Scattering of massless particles: scalars, gluons and gravitons, [JHEP **07**, 033 \(2014\)](#)
- [15] Stephen P. Jordan, Keith S. M. Lee, John Preskill, Quantum algorithms for quantum field theories, [Science **336**, 1130–1133 \(2012\)](#)
- [16] John Preskill, Quantum computing in the NISQ era and beyond, [Quantum **2**, 79 \(2018\)](#)
- [17] Natalie Klco et al., Quantum-classical computation of Schwinger model dynamics, [Phys. Rev. A **98**, 032331 \(2018\)](#)
- [18] Christian W. Bauer et al., Quantum simulation for high-energy physics, [PRX Quantum **4**, 027001 \(2023\)](#)
- [19] Eric Bashore, Caleb Bashore et al., Quantum Algorithm for MHV Scattering Amplitudes, [SciPost Phys.,114-20 ,SciPost , \(2026\)](#)
- [20] Yakir Aharonov, Luiz Davidovich, Nicim Zagury, Quantum random walks, [Phys. Rev. A **48**, 1687–1690 \(1993\)](#)
- [21] David A. Meyer, From quantum cellular automata to quantum lattice gases, [J. Stat. Phys. **85**, 551–574 \(1996\)](#)
- [22] Andris Ambainis, Quantum walks and their algorithmic applications, [Int. J. Quantum Inf. **1**, 507–518 \(2003\)](#)
- [23] Julia Kempe, Quantum random walks: an introductory overview, [Contemp. Phys. **44**, 307–327 \(2003\)](#)
- [24] Salvador E. Venegas-Andraca, Quantum walks: a comprehensive review, [Quantum Inf. Process. **11**, 1015–1106 \(2012\)](#)
- [25] Renato Portugal, Quantum Walks and Search Algorithms, [Springer \(2013\)](#)
- [26] Mallick, A., Chandrashekar, C. Dirac Cellular Automaton from Split-step Quantum Walk. [Sci Rep **6**, 25779 \(2016\)](#)
- [27] Chandrashekar, C. Two-component Dirac-like Hamiltonian for generating quantum walk on one-, two- and three-dimensional lattices. [Sci Rep **3**, 2829 \(2013\)](#)
- [28] Arindam Mallick, Sanjoy Mandal, Anirban Karan and C M Chandrashekar , Simulating Dirac Hamiltonian in curved space-time by split-step quantum walk, [Journal of Physics Communications **2399-6528** \(2019\)](#)
- [29] Mallick, A., Mandal, S. & Chandrashekar, C.M. Neutrino oscillations in discrete-time quantum walk framework, [Eur. Phys. J. C **77**, 85 \(2017\)](#)
- [30] Sahu, H., Chandrashekar, C.M. Open system approach to neutrino oscillations in a quantum walk framework. [Quantum Inf Process **23**, 7 \(2024\)](#).
- [31] Huerta Alderete, C., Singh, S., Nguyen, N.H. et al. Quantum walks and Dirac cellular automata on a programmable trapped-ion quantum computer, [Nat Commun **11**, 3720 \(2020\)](#).
- [32] Kumar, N. Pradeep and Balu, Radhakrishnan and Laflamme, Raymond and Chandrashekar, C. M., Bounds on the dynamics of periodic quantum walks and emergence of the gapless and gapped Dirac equation, [Phys. Rev. A. **97.012116** \(2018\)](#).
- [33] Sengupta, Kanad and Dinesh, S.P. and Shafi, K. Muhammed and Asokan, Soumya and Chandrashekar, C.M, Experimental realization of universal quantum gates and a six-qubit entangled state using a photonic quantum walk, [Phys. Rev. Appl. \(2025\)](#).
- [34] Karl Kraus, States, Effects and Operations, [Springer \(1983\)](#)
- [35] Breuer, Heinz-Peter, and Francesco Petruccione, The Theory of Open Quantum Systems ([Oxford, 2007; online edn, Oxford Academic, 1 Feb. 2010](#)).
- [36] Michael A. Nielsen, Isaac L. Chuang, Quantum Computation and Quantum Information, [Cambridge University Press \(2010\)](#)
- [37] Stephane Attal, Francesco Petruccione, Christophe Sabot, Ilya Sinayskiy, Open quantum random walks, [J. Stat. Phys. **147**, 832–852 \(2012\)](#)
- [38] Ilya Sinayskiy, Francesco Petruccione, Open quantum walks: a short introduction, [Int. J. Quantum Inf. **10**, 1240004 \(2012\)](#)
- [39] Peter W. Shor, Algorithms for quantum computation: discrete logarithms and factoring, [Proc. FOCS, **124–134** \(1994\)](#)
- [40] Don Coppersmith, An approximate Fourier transform useful in quantum factoring, IBM Research Report RC 19642 (1994); [arXiv:quant-ph/0201067](#)

SUPPLEMENTARY MATERIAL

This supplementary material provides additional implementation details and numerical data supporting the results presented in the main text. In particular, we present the bijectivity proof for the shift operator, summarize the basis-indexing conventions, construction of the local coin and shift operators, implementation of the weighted collection operator, verification of the Kraus channel, and additional numerical results beyond those reported in the main manuscript.

Appendix A: Bijectivity of the Shift Operator

We provide additional detail for the bijectivity argument (Proposition 1).

Under the global edge-labeling convention, coin value k corresponds to particle $p = k+2$. For each sector k , the basis states $V \times \{k\}$ are partitioned into F_k (forward), L_k (self-loop), and D_k (displaced); see (19)–(21).

a. Source and target classification. The three rules produce three disjoint sets of images:

1. *Forward images:* $\text{Im}(F_k) = \{(u, k) : u \neq r, \kappa(u) = k\}$, i.e. all non-root nodes whose last element is particle $k+2$. The forward rule is injective (each such node has a unique parent).
2. *Self-loop images:* $\text{Im}(L_k) = L_k$ (each state maps to itself). These satisfy $k \neq \kappa(v)$, so they are disjoint from forward images (which satisfy $\kappa(u) = k$).
3. *Displaced images:* $\text{Im}(D_k) = \mathcal{U}_k$, the uncovered targets. By definition, \mathcal{U}_k contains neither forward images nor self-loop states, so this set is disjoint from the other two.

Since the three image sets are disjoint and each rule is injective on its domain, τ is injective on $V \times \{k\}$. By the pigeonhole principle on a finite set, injectivity implies bijectivity. Since this holds for every k , τ is a permutation on the full basis and S is unitary.

Appendix B: Basis Indexing Convention

The quantum walk is implemented on the Hilbert space

$$\mathcal{H} = \mathcal{H}_{\text{pos}} \otimes \mathcal{H}_{\text{coin}}, \quad (\text{B1})$$

with

$$\dim(\mathcal{H}_{\text{pos}}) = 16, \quad \dim(\mathcal{H}_{\text{coin}}) = 3. \quad (\text{B2})$$

The computational basis is ordered according to

$$|0, 0\rangle, |0, 1\rangle, |0, 2\rangle, |1, 0\rangle, |1, 1\rangle, |1, 2\rangle, \dots, |15, 2\rangle, \quad (\text{B3})$$

resulting in a total Hilbert-space dimension of 48.

Table III summarizes the mapping between node labels and permutation sectors.

Node Index	Permutation Sector
0	(1)
1	(12)
2	(13)
3	(14)
4	(123)
5	(124)
6	(132)
7	(134)
8	(142)
9	(143)
10	(1234)
11	(1243)
12	(1324)
13	(1342)
14	(1423)
15	(1432)

TABLE III: Basis indexing convention used in the numerical implementation.

Appendix C: Classification of Basis States in the Shift Operator

For the four-gluon permutation tree, every basis state $|v, k\rangle \in V \times \{0, 1, 2\}$ belongs uniquely to one of the three subsets F_k , L_k , or D_k introduced in Sec. III D. The classification is determined entirely by the remaining-particle set $R(v)$, the incoming coin label $\kappa(v)$, and whether the node is terminal. Table IV lists the resulting partition explicitly for all sixteen nodes of the permutation tree.

The cardinalities of the three subsets for each coin sector are summarized in Table V. As expected,

$$|F_k| + |L_k| + |D_k| = |V|, \quad (\text{C1})$$

for every coin value k , confirming that the three subsets form a partition of the node set in each coin sector.

Appendix D: Quantum Fourier Transform

For the three-dimensional coin space used in the four-gluon example, the quantum Fourier transform is

$$U_{\text{QFT}} = \frac{1}{\sqrt{3}} \begin{pmatrix} 1 & 1 & 1 \\ 1 & \omega & \omega^2 \\ 1 & \omega^2 & \omega \end{pmatrix}, \quad (\text{D1})$$

TABLE IV: Classification of the basis states for the four-gluon permutation tree. Here F , L , and D denote the forward, loop and displaced subsets, respectively.

Node v	$k = 0$	$k = 1$	$k = 2$
(1)	F	F	F
(1, 2)	D	F	F
(1, 3)	F	D	F
(1, 4)	F	F	D
(1, 2, 3)	L	D	F
(1, 2, 4)	L	F	D
(1, 3, 2)	D	L	F
(1, 3, 4)	F	L	D
(1, 4, 2)	D	F	L
(1, 4, 3)	F	D	L
(1, 2, 3, 4)	D	D	D
(1, 2, 4, 3)	D	D	D
(1, 3, 2, 4)	D	D	D
(1, 3, 4, 2)	D	D	D
(1, 4, 2, 3)	D	D	D
(1, 4, 3, 2)	D	D	D

TABLE V: Cardinalities of the three subsets for the four-gluon example.

Subset	$k = 0$	$k = 1$	$k = 2$
F_k	6	6	6
L_k	3	3	3
D_k	7	7	7
Total	16	16	16

where

$$\omega = e^{2\pi i/3}. \quad (\text{D2})$$

After application of the collection operator, the Fourier transform generates the interference required for reconstruction of the color-ordered scattering amplitude.

Appendix E: Five-Gluon Permutation Graph

The main text focuses on the four-gluon scattering process. To illustrate the scalability of the framework, Fig. 9 shows the corresponding graph for the five-gluon case.

Appendix F: Growth of the Permutation Tree

For an n -gluon scattering process, the permutation tree is generated by successively inserting a new particle into all admissible positions of the existing orderings. The number of terminal permutation sectors is therefore

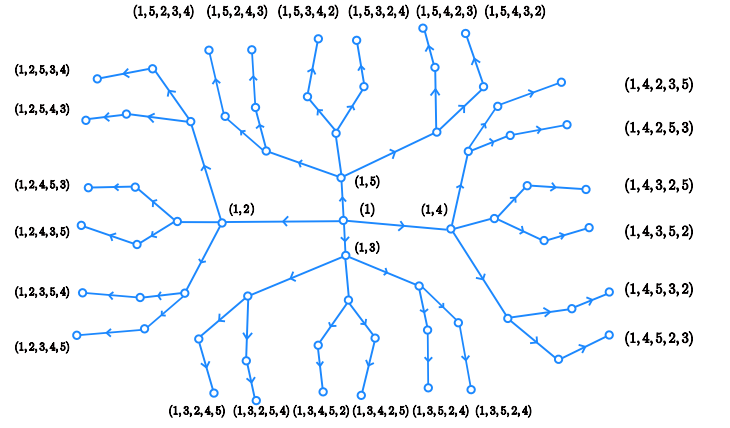


FIG. 9: Permutation graph for the five-gluon scattering process. The graph is generated using the same recursive insertion procedure used for the four-gluon example and illustrates the growth of the permutation-tree structure with increasing multiplicity.

$$N_{\text{term}} = (n - 1)!. \quad (\text{F1})$$

The total number of nodes in the permutation tree is

$$g(n) = \sum_{k=0}^{n-1} \frac{(n-1)!}{k!}, \quad (\text{F2})$$

while the Hilbert-space dimension of the coined quantum walk is

$$D(n) = (n - 1)g(n), \quad (\text{F3})$$

where the factor $(n - 1)$ arises from the coin dimension.

Table VI summarizes the scaling of the permutation-tree representation and the corresponding quantum-walk Hilbert space.

n	$g(n)$	$D(n)$
4	16	48
5	65	260
6	326	1630

TABLE VI: Growth of the permutation-tree graph and the corresponding quantum-walk Hilbert-space dimension.

Appendix G: Derivation of the Quantum-Walk State

We derive the explicit form of the quantum-walk state generated by $(SC)^{n-1}|\psi_0\rangle$ and establish its correspondence to the Parke–Taylor denominator. The derivation is fully consistent with the coin condition (17) of the main

text: the physically relevant column of C_v is always column $\kappa(v)$, equal to the coin value carried by the walker upon arriving at v .

a. *Step 0 (Initialization).*

$$|\psi_0\rangle = |(1)\rangle \otimes |0\rangle. \quad (\text{E1})$$

The root has $\kappa(r) = 0$ by convention, so the coin operator $C_{(1)}$ is applied through its column 0.

b. *Step 1.*

$$C|\psi_0\rangle = \sum_{k_1=0}^{d-1} (C_{(1)})_{k_1,0} |(1)\rangle \otimes |k_1\rangle, \quad (\text{E2})$$

$$SC|\psi_0\rangle = \sum_{k_1=0}^{d-1} (C_{(1)})_{k_1,0} |(1, k_1+2)\rangle \otimes |k_1\rangle, \quad (\text{E3})$$

where the shift appends particle k_1+2 (the particle corresponding to coin k_1 under the global map). The child $(1, k_1+2)$ has $\kappa((1, k_1+2)) = c(k_1+2) = k_1$.

c. *General step m .* After m applications, with $v_0 = r$ and $v_s = (1, k_1+2, \dots, k_s+2)$ for $s \geq 1$:

$$(SC)^m |\psi_0\rangle = \sum_{k_1, \dots, k_m} \left(\prod_{s=1}^m (C_{v_{s-1}})_{k_s, \kappa(v_{s-1})} \right) |v_m\rangle \otimes |k_m\rangle. \quad (\text{E4})$$

The column index $\kappa(v_{s-1}) = k_{s-1}$ (where $k_0 = 0$) is the coin label with which the walker arrived at v_{s-1} . Under the global convention, $k_{s-1} = c(\sigma(s)) = \sigma(s) - 2$ for $s \geq 2$ and $k_0 = 0$ for the root. This is guaranteed by the shift operator, which preserves the coin label: the walker arrives at v_{s-1} in state $|k_{s-1}\rangle$, the coin operator maps $|k_{s-1}\rangle$ through column $\kappa(v_{s-1}) = k_{s-1}$ of $C_{v_{s-1}}$, and the shift routes to the child indexed by the new coin value $k_s = c(\sigma(s+1)) = \sigma(s+1) - 2$.

d. *Terminal state ($m = n - 1$).* Each sequence (k_1, \dots, k_{n-1}) with $k_s \in \{0, \dots, |R(v_{s-1})| - 1\}$ specifies a unique root-to-terminal path and hence a unique permutation $\sigma = (1, \sigma(2), \dots, \sigma(n)) \in S_{n-1}$. The map from valid coin sequences to permutations is a bijection. Re-indexing:

$$|\psi_{\text{fin}}\rangle = \sum_{\sigma \in S_{n-1}} \psi_\sigma |\sigma\rangle \otimes |k_\sigma\rangle, \quad (\text{E5})$$

where $k_\sigma = k_{n-1} = c(\sigma(n)) = \sigma(n) - 2$ is the global coin label of the last appended particle.

e. *Explicit path amplitude.* From condition (17) and the global coin map (7), at step s the relevant matrix element is

$$(C_{v_{s-1}})_{c(\sigma(s+1)), \kappa(v_{s-1})} = \tilde{v}_{v_{s-1}, \sigma(s+1)} = \frac{1}{\alpha_{v_{s-1}}} \cdot \frac{1}{\langle \sigma(s) \sigma(s+1) \rangle}, \quad \text{where} \quad (\text{E6})$$

where the row index $c(\sigma(s+1)) = \sigma(s+1) - 2$ is the global coin label of the appended particle, and $\ell(v_{s-1}) = \sigma(s)$.

Taking the product over $s = 1, \dots, n - 1$:

$$\psi_\sigma = \left(\prod_{r=1}^{n-1} \frac{1}{\alpha_{\sigma(r)}} \right) \cdot \frac{1}{\langle 1 \sigma(2) \rangle \langle \sigma(2) \sigma(3) \rangle \cdots \langle \sigma(n) 1 \rangle}. \quad (\text{E7})$$

Comparing with

$$A_\sigma = \frac{\langle 1\tilde{k} \rangle^4}{\langle 1 \sigma(2) \rangle \langle \sigma(2) \sigma(3) \rangle \cdots \langle \sigma(n) 1 \rangle}, \quad (\text{E8})$$

yields

$$\boxed{\psi_\sigma = \frac{\langle \sigma(n) 1 \rangle}{\langle 1\tilde{k} \rangle^4 \prod_{r=1}^{n-1} \alpha_{\sigma(r)}} A_\sigma.} \quad (\text{E9})$$

The coined quantum walk thus reproduces the ordered Parke–Taylor denominator through coherent evolution on the permutation tree, with the proportionality constant explicitly known.

Appendix H: Derivation of the Kraus-Channel Representation

The final coherent walk state derived in Appendix G is

$$|\psi_{\text{fin}}\rangle = \sum_{\sigma \in \mathcal{T}} \psi_\sigma |\sigma\rangle \otimes |k_\sigma\rangle, \quad (\text{H1})$$

where

$$\psi_\sigma = A_\sigma \frac{\langle \sigma(n) 1 \rangle}{\langle 1\tilde{k} \rangle^4 \prod_r \alpha_{\sigma(r)}}. \quad (\text{H2})$$

The corresponding density operator is

$$\rho = |\psi_{\text{fin}}\rangle \langle \psi_{\text{fin}}|. \quad (\text{H3})$$

To isolate the contribution of each permutation sector we introduce the family of Kraus operators

$$K_\sigma = c_\sigma |\sigma\rangle \langle \sigma| \otimes I_{\text{coin}}, \quad (\text{H4})$$

with

$$c_\sigma = \frac{\langle 1\tilde{k} \rangle^4}{\langle \sigma(n) 1 \rangle} \frac{1}{M}, \quad (\text{F5})$$

$$M = \max_{\sigma} \left| \frac{\langle 1\tilde{k} \rangle^4}{\langle \sigma(n) 1 \rangle} \right|. \quad (\text{H5})$$

The normalization guarantees

$$|c_\sigma| \leq 1, \quad (\text{H6})$$

and therefore

$$\begin{aligned} \sum_\sigma K_\sigma^\dagger K_\sigma &= \sum_\sigma |c_\sigma|^2 |\sigma\rangle\langle\sigma| \otimes I_{\text{coin}} \\ &\leq I, \end{aligned} \quad (\text{H7})$$

showing that the resulting map is completely positive and trace non-increasing.

The quantum channel acts as

$$\rho' = \sum_\sigma K_\sigma \rho K_\sigma^\dagger. \quad (\text{F8})$$

Since $K_\sigma = c_\sigma |\sigma\rangle\langle\sigma| \otimes I_{\text{coin}}$, applying K_σ from the left projects the position register onto $|\sigma\rangle$, and applying K_σ^\dagger from the right projects onto $\langle\sigma|$:

$$K_\sigma (|\sigma'\rangle\langle\sigma''| \otimes |k\rangle\langle k'|) K_\sigma^\dagger = |c_\sigma|^2 \delta_{\sigma\sigma'} \delta_{\sigma\sigma''} |\sigma\rangle\langle\sigma| \otimes |k\rangle\langle k'|. \quad (\text{F9})$$

Substituting $\rho = \sum_{\sigma',\sigma''} \psi_{\sigma'} \psi_{\sigma''}^* |\sigma'\rangle\langle\sigma''| \otimes |k_{\sigma'}\rangle\langle k_{\sigma''}|$ and summing over σ :

$$\rho' = \sum_\sigma |c_\sigma|^2 |\psi_\sigma|^2 |\sigma\rangle\langle\sigma| \otimes |k_\sigma\rangle\langle k_\sigma|. \quad (\text{F10})$$

The coin degree of freedom is not projected by K_σ (it contains I_{coin}); the off-diagonal coin terms $|k_{\sigma'}\rangle\langle k_{\sigma''}|$ with $\sigma' \neq \sigma''$ vanish because the position orthogonality $\delta_{\sigma\sigma'} \delta_{\sigma\sigma''}$ forces $\sigma' = \sigma'' = \sigma$, fixing the coin label to k_σ . Using (F5) and (E9):

$$|c_\sigma|^2 |\psi_\sigma|^2 = \frac{|A_\sigma|^2}{|M|^2 \prod_r |\alpha_{\sigma(r)}|^2}, \quad (\text{F11})$$

so that $(\rho')_{\sigma\sigma} \propto |A_\sigma|^2$.

Consequently,

$$(\rho')_{\sigma\sigma} = \frac{|A_\sigma|^2}{|M|^2 \prod_r |\alpha_{\sigma(r)}|^2}, \quad (\text{H8})$$

and, using the proportionality relation (31),

$$(\rho')_{\sigma\sigma} \propto |A_\sigma|^2. \quad (\text{H9})$$

Hence the Kraus-channel construction extracts the squared Parke–Taylor contribution associated with each terminal permutation sector while preserving complete positivity and trace non-increase.

Appendix I: Construction of the Weighted Collection Operator

The final coherent quantum-walk state obtained in Appendix G contains the color-ordered Parke–Taylor contributions distributed over the terminal nodes of the permutation tree. In order to reconstruct the complete scattering amplitude, these terminal sectors must be coherently combined while preserving their relative amplitudes. For this purpose we introduce the weighted collection operator

$$W^T = \sum_{j_{n-1} \in V \setminus \{R\}} \cdots \sum_{j_1 \in V \setminus \{R\}} C_{j_{n-1}, R}^{n-1} C_{j_{n-2}, R}^{n-2} \cdots C_{j_1, R}^1, \quad (\text{I1})$$

where

$$C_{j_k, R}^i = a_\sigma |R\rangle\langle j_k| \otimes |i\rangle\langle i| + \sum_{\tilde{i} \neq i} |j_k\rangle\langle j_k| \otimes |\tilde{i}\rangle\langle \tilde{i}|. \quad (\text{I2})$$

The first term transfers the walker from the terminal node j_k to the common reference node R conditioned on the coin state i , while the remaining coin components are left unchanged.

The coefficient a_σ is associated with the complete terminal permutation

$$\sigma = (j_1, j_2, \dots, j_{n-1}),$$

and contains the corresponding color and kinematic information,

$$a_\sigma = \frac{\text{Tr} \left(T^{(\sigma')_0} T^{(\sigma')_2} \dots T^{(\sigma')_{n-1}} \right) \frac{\langle 1\tilde{k} \rangle^4}{\langle \sigma(n) 1 \rangle}}{\mathcal{N}}, \quad (\text{I3})$$

where σ' denotes the corresponding color ordering.

The normalization constant

$$\mathcal{N} = \max_\sigma \left| \text{Tr} (T^{a_1} T^{a_{\sigma(2)}} \dots T^{a_{\sigma(n)}}) \frac{\langle 1\tilde{k} \rangle^4}{\langle \sigma(n) 1 \rangle} \right| \quad (\text{I4})$$

is chosen so that

$$|a_\sigma| \leq 1, \quad (\text{I5})$$

ensuring that the collection operator remains bounded.

We evaluate the action of the weighted collection operator on the terminal quantum-walk state

$$|\psi_{\text{fin}}\rangle = \sum_{\sigma \in \mathcal{T}} A_\sigma \frac{\langle \sigma(n) 1 \rangle}{\langle 1\tilde{k} \rangle^4 \prod_r \alpha_{\sigma(r)}} |\sigma\rangle \otimes |k_\sigma\rangle. \quad (\text{I6})$$

Because the coin states form an orthonormal basis,

$$\langle i|\tilde{i}\rangle = \delta_{i\tilde{i}},$$

all operator sequences whose coin conditioning is inconsistent with the terminal path vanish. Consequently only the sequence associated with the permutation σ contributes,

$$\tilde{C}_\sigma = C_{j_{n-1},R}^{n-1} \cdots C_{j_1,R}^1 = a_\sigma |R\rangle \langle \sigma| \otimes |k_\sigma\rangle \langle k_\sigma|. \quad (\text{I7})$$

The action of the complete collection operator is therefore

$$W^T |\psi_{\text{fin}}\rangle = \sum_{\sigma \in \mathcal{T}} a_\sigma A_\sigma \frac{\langle \sigma(n) 1 \rangle}{\langle 1\tilde{k} \rangle^4 \prod_r \alpha_{\sigma(r)}} \times |R\rangle \otimes |k_\sigma\rangle. \quad (\text{I8})$$

Substituting the explicit expression for a_σ yields

$$W^T |\psi_{\text{fin}}\rangle = \sum_{\sigma \in \mathcal{T}} \frac{\text{Tr} \left(T^{(\sigma')_0} T^{(\sigma')_2} \dots T^{(\sigma')_{n-1}} \right)}{\mathcal{N}} \times \frac{A_\sigma}{\prod_r \alpha_{\sigma(r)}} |R\rangle \otimes |k_\sigma\rangle. \quad (\text{I9})$$

Thus all terminal sectors are coherently collected at the reference node while the interference information is preserved entirely in the coin degrees of freedom.

Appendix J: Quantum Fourier Transform and Amplitude Reconstruction

The collected state obtained in Appendix I has the form

$$W^T |\psi_{\text{fin}}\rangle = |R\rangle \otimes \sum_{\sigma \in \mathcal{T}} c_\sigma |k_\sigma\rangle, \quad (\text{J1})$$

where

$$c_\sigma = \frac{\text{Tr} \left(T^{(\sigma')_0} T^{(\sigma')_2} \dots T^{(\sigma')_{n-1}} \right)}{\mathcal{N}} \frac{A_\sigma}{\prod_r \alpha_{\sigma(r)}}. \quad (\text{J2})$$

The Quantum Fourier Transform [36, 40] on the $(n-1)$ -dimensional coin space is

$$U_{\text{QFT}} = \frac{1}{\sqrt{n-1}} \sum_{j,k=0}^{n-2} e^{2\pi i j k / (n-1)} |j\rangle \langle k|. \quad (\text{J3})$$

Applying the QFT gives

$$(\mathbb{I} \otimes U_{\text{QFT}}) W^T |\psi_{\text{fin}}\rangle = |R\rangle \otimes \sum_{\sigma} c_\sigma U_{\text{QFT}} |k_\sigma\rangle. \quad (\text{J4})$$

Finally, projection onto the Fourier vacuum state produces

$$\mathcal{M} = (\mathbb{I} \otimes \langle 0|) (\mathbb{I} \otimes U_{\text{QFT}}) W^T |\psi_{\text{fin}}\rangle. \quad (\text{J5})$$

Since

$$\langle 0|U_{\text{QFT}}|k_\sigma\rangle = \frac{1}{\sqrt{n-1}}, \quad (\text{J6})$$

the reconstructed amplitude becomes

$$\mathcal{M} = \frac{1}{\sqrt{n-1}} \sum_{\sigma \in \mathcal{T}} \frac{\text{Tr} (T^{a_1} T^{a_{\sigma(2)}} \dots T^{a_{\sigma(n)}})}{\mathcal{N}} \frac{A_\sigma}{\prod_r \alpha_{\sigma(r)}}. \quad (\text{J7})$$

Therefore,

$$|\mathcal{M}|^2 \propto \sum_{\sigma \in \mathcal{S}_{n-1}} \text{Tr} (T^{a_1} T^{a_{\sigma(2)}} \dots T^{a_{\sigma(n)}}) A_\sigma|^2, \quad (\text{J8})$$

demonstrating that the weighted collection operator together with the Quantum Fourier Transform reconstructs the coherent color-decomposed scattering amplitude from the quantum-walk state.

Appendix K: Verification of the Kraus Channel

The extraction procedure introduced in the main text is implemented through a set of Kraus operators $\{K_i\}$ acting on the terminal permutation sectors. For the resulting map to represent a physically valid quantum operation, the Kraus operators must satisfy the trace non-increasing condition

$$\sum_i K_i^\dagger K_i \leq I. \quad (\text{K1})$$

This condition guarantees complete positivity and ensures that the channel corresponds to a valid measurement-induced extraction process.

To verify this property numerically, we construct the operator

$$\Lambda = \sum_i K_i^\dagger K_i, \quad (\text{K2})$$

and compute its spectrum. The extremal eigenvalues are found to be

$$\lambda_{\max}(\Lambda) = 1, \quad \lambda_{\min}(\Lambda) = 0. \quad (\text{K3})$$

Since all eigenvalues satisfy

$$0 \leq \lambda_i \leq 1, \quad (\text{K4})$$

the operator Λ is positive semidefinite and bounded above by the identity operator. Consequently,

$$\Lambda \leq I, \quad (\text{K5})$$

which confirms that the Kraus map used in the numerical simulations is completely positive and trace non-increasing.

This verification establishes the consistency of the extraction channel employed to isolate the sector-resolved Parke–Taylor contributions from the coherent quantum-walk state.

Appendix L: Additional Numerical Results

This section contains the complete numerical data used for validation of the quantum-walk reconstruction procedure, including additional kinematic configurations, reconstructed amplitudes, and relative errors.

Appendix M: Comparison with Quantum Circuit Approach

We now compare the present quantum-walk-based construction with the quantum circuit algorithm for MHV amplitudes introduced in Ref. [19]. While both approaches aim to reconstruct color-ordered scattering amplitudes using quantum-information-inspired frameworks, they differ substantially in their physical interpretation, encoding strategy, and mechanism for generating interference between permutation sectors.

Aspect	Quantum Walk Construction (This Work)	Quantum Circuit Algorithm (Ref. [19])
Basic framework	Permutation tree with coined quantum walk dynamics	Quantum circuit acting on structured quantum registers
Underlying structure	Directed graph whose paths encode color-ordered sectors	Register-based encoding of permutations and particle data
Hilbert space	Position space (tree nodes) \otimes coin space	Permutation, momentum, helicity, and color registers
Generation of permutations	Generated dynamically through coherent propagation on the permutation tree	Prepared explicitly as a superposition over permutation basis states
Kinematic structure	Built locally through edge-dependent transition amplitudes	Implemented through controlled helicity-dependent gates
Color structure	Introduced through weighted collection coefficients a_σ	Implemented through dedicated color operators U_C
Physical interpretation	Scattering amplitudes emerge from coherent quantum transport and path interference	Scattering amplitudes are encoded through structured circuit operations
Role of the coin system	Labels outgoing branches and stores interference information between paths	No direct analogue; interference occurs through global circuit operations
Interference mechanism	Generated through coherent recombination at the reference node and coin-space mixing	Generated globally through the Quantum Fourier Transform (QFT)
Amplitude reconstruction	Weighted collection operator followed by QFT and projection	QFT followed by projection onto a reference ancilla state
Extraction of $ A_\sigma ^2$	Obtained through Kraus operators acting on terminal permutation sectors	Obtained through measurement of encoded amplitude registers
Open quantum systems interpretation	Explicitly formulated using Kraus operators and completely positive maps	Primarily unitary circuit formulation
Normalization strategy	Local normalization of transition weights using bounded coefficients	Global normalization using ancilla-assisted unitary embedding
Permutation encoding	Encoded geometrically as root-to-terminal paths on the permutation tree	Encoded algebraically in permutation registers
Scalability structure	Factorial number of terminal paths represented through graph connectivity; Hilbert-space dimension $D(n) = (n-1) \sum_{k=0}^{n-1} (n-1)!/k!$	Permutation sectors encoded using logarithmic register scaling; $O(n \log n)$ qubits
Number of coherent steps	$n-1$ applications of the walk operator $U = SC$	$O(n!)$ controlled gate operations
Non-unitary operations	Kraus channel (sector extraction); weighted collection operator W^T (requires ancilla-assisted dilation for physical implementation)	Ancilla-assisted unitary embedding for non-unitary amplitude factors
Key conceptual insight	Scattering amplitudes arise dynamically from coherent evolution on permutation graphs	Scattering amplitudes are reconstructed through structured quantum circuit synthesis

TABLE VII: Comparison between the quantum-walk construction developed in this work and the quantum circuit algorithm for MHV scattering amplitudes introduced in Ref. [19]. While both approaches reconstruct coherent sums over color-ordered sectors, the present framework interprets the scattering process as quantum transport and interference on a permutation graph.